arXiv:0704.0735v2 [astro-ph] 11 Apr 2007

# The HELLAS2XMM survey

## X. The bolometric output of luminous obscured quasars: The Spitzer perspective

F. Pozzi,[1,2] C. Vignali,[1,2] A. Comastri,[2] L. Pozzetti,[2] M. Mignoli,[2] C. Gruppioni,[2] G. Zamorani,[2] C. Lari,[3] F. Civano,[1,2] M. Brusa,[4] F. Fiore,[5] R. Maiolino,[5] and F. La Franca[6]

[1] Dipartimento di Astronomia, Università degli Studi di Bologna, Via Ranzani 1, I–40127 Bologna, Italy
[2] INAF — Osservatorio Astronomico di Bologna, Via Ranzani 1, I–40127 Bologna, Italy
[3] INAF — Istituto di Radioastronomia (IRA), Via Gobetti 101, I–40129 Bologna, Italy
[4] Max Planck Institut für Extraterrestrische Physik (MPE), Giessenbachstrasse 1, D-85748 Garching bei München, Germany
[5] INAF — Osservatorio Astronomico di Roma, Via Frascati 33, I–00040 Monteporzio-Catone (RM), Italy
[6] Dipartimento di Fisica, Università degli Studi Roma Tre, Via della Vasca Navale 84, I–00146 Roma, Italy

**ABSTRACT**

*Aims.* We aim at estimating the spectral energy distributions (SEDs) and the physical parameters related to the black holes harbored in eight high X-ray-to-optical ($F_X/F_R$ >10) obscured quasars at $z > 0.9$ selected in the 2–10 keV band from the HELLAS2XMM survey.
*Methods.* We use IRAC and MIPS 24 $\mu$m observations, along with optical and $K_s$-band photometry, to obtain the SEDs of the sources. The observed SEDs are modeled using a combination of an elliptical template and torus emission (using the phenomenological templates of Silva et al. 2004) for six sources associated with passive galaxies; for two point-like sources, the empirical SEDs of red quasars are adopted. The bolometric luminosities and the $M_{BH} - L_K$ relation are used to provide an estimate of the masses and Eddington ratios of the black holes residing in these AGN.
*Results.* All of our sources are detected in the IRAC and MIPS (at 24 $\mu$m) bands. The SED modeling described above is in good agreement with the observed near- and mid-infrared data. The derived bolometric luminosities are in the range $\approx 10^{45} - 10^{47}$ erg s$^{-1}$, and the median 2–10 keV bolometric correction is $\approx$25, consistent with the widely adopted value derived by Elvis et al. (1994). For the objects with elliptical-like profiles in the $K_s$ band, we derive high stellar masses $(0.8 - 6.2) \times 10^{11}$ M$_\odot$, black hole masses in the range $(0.2 - 2.5) \times 10^9$ M$_\odot$, and Eddington ratios $L/L_{Edd} < 0.1$, suggesting a low-accretion phase.

**Key words.** quasars: general — galaxies: nuclei — galaxies: active

## 1. Introduction

Hard X-ray surveys have clearly revealed the important role played by obscured Active Galactic Nuclei (AGN) to reproduce the cosmic X-ray background (XRB; e.g., Comastri et al. 1995) and have provided evidence that a significant fraction of the accretion-driven energy density in the Universe resides in obscured X-ray sources (e.g., Barger et al. 2005; Hopkins et al. 2006; Hickox & Markevitch 2006).

Until recently, the limited information on the broad-band emission of the counterparts of obscured X-ray sources prevented a reliable determination of their bolometric luminosities. The lack of a proper knowledge of the spectral energy distributions (SEDs) of obscured sources has led many authors to adopt, in the computation of the bolometric luminosities, the average value derived by Elvis et al. (1994), although in that work the sample comprises mostly local unabsorbed quasars. By the current work, we aim at providing a robust estimate of the bolometric luminosity for obscured sources, which is an essential parameter to derive the cosmic mass density of supermassive black holes (SMBHs, i.e., following the Soltan 1982 approach). A reliable estimate of the bolometric luminosity of obscured AGN is typically limited by the actual capabilities of disentangling the nuclear emission (related to the accretion processes) from that of the host galaxy which, unlike for unabsorbed quasars, often dominates at optical and near-infrared (near-IR) bands.

A significant fraction of high-redshift, luminous obscured AGN (the so-called Type 2 quasars) may have escaped spectroscopic identification due to their faint optical counterparts, thus preventing current studies from an accurate sampling of obscured sources. Mid-infrared (mid-IR) observations appear

**Table 1.** Properties of our targets

| Source Id. | 2–10 keV flux[†] ($10^{-14}$ erg cm$^{-2}$ s$^{-1}$) | $R$ | $K_s$ | Morph($K_s$) | X/O | $z$ |
|---|---|---|---|---|---|---|
| Abell 2690#75 | 3.30 | 24.60 | 18.33 | E | 1.86 | 2.13[a] |
| PKS 0312−77#36 | 1.90 | 24.70 | 19.13 | E | 1.66 | – |
| PKS 0537−28#91 | 4.20 | 23.70 | 18.99 | E | 1.60 | – |
| PKS 0537−28#54 | 2.10 | 25.10 | 18.91 | E | 1.86 | – |
| PKS 0537−28#111 | 2.10 | 24.50 | 17.64 | E | 1.62 | – |
| Abell 2690#29 | 2.80 | 25.10 | 17.67 | P | 1.99 | 2.08[b] |
| PKS 0312−77#45 | 2.80 | 24.40 | 18.62 | P | 1.71 | – |
| BPM 16274#69 | 2.27 | 24.08 | 17.87 | E | 1.49 | 1.35[b] |

[†] 2-10 kev X-ray fluxes from Perola et al. (2004).
[a] Tentative spectroscopic redshift from near-IR spectroscopic observations (Maiolino et al. 2006).
[b] Spectroscopic redshift from near-IR spectroscopic observations (Maiolino et al. 2006).

to be fundamental for this class of objects, since they are only marginally affected by dust obscuration and are able to recover the nuclear emission. With mid-IR observations, we expect to reveal the nuclear radiation re-processed by the torus of the obscured active nuclei, which are often recognized as such by means of their X-ray emission only. For these sources, the soft X-ray emission, which is photo-electrically absorbed by the gas, and the optical emission, extincted by the dusty circumnuclear medium, are expected to be downgraded in energy and to emerge as thermally reprocessed radiation in the IR at wavelengths in the range between a few and a few hundred $\mu$m (Granato et al. 1997).

The potentialities of mid-IR observations were firstly shown by Fadda et al. (2002), who detected with *ISOCAM* at 15 $\mu$m about two-thirds of the X-ray sources detected in the 5–10 keV band in the XMM-*Newton* Lockman Hole survey. A similar high detection rate at 24 $\mu$m has been recently reported by Rigby et al. (2004) and Franceschini et al. (2005) studying the *Spitzer* counterparts of the *Chandra* sources in the CDF-S and in the ELAIS-N1 field, respectively, within the SWIRE survey (Lonsdale et al. 2004).

In this context, a new interesting class of objects is emerging from the current X-ray surveys: these sources are characterized by a high (>1) X-ray-to-optical flux ratio (hereafter X/O)[1]; for comparison, unobscured Type 1 AGN have a broad distribution peaked at X/O≈0. Objects with X/O ≳1 are about 20% of the hard X-ray selected sources, and the fraction of these sources seems to remain constant over ≈ 3 decades of X-ray flux (Comastri & Fiore 2004). By definition, sources with high X/O are among the faintest sources in the optical band. In the shallow, large-area X-ray surveys (e.g., the HELLAS2XMM survey, with $F_{2-10 \ keV} > 10^{-14}$ erg cm$^{-2}$ s$^{-1}$ over ≈ 3 deg$^2$; Baldi et al. 2002), where the identification of a sizable sample of sources with X/O>1 has been possible (e.g., Fiore et al. 2003), the X/O selection criterion has proven to be effective in selecting Type 2 quasars at high redshifts.

We have performed a pilot program to study with *Spitzer* a sample of eight sources selected in the 2–10 keV band from the HELLAS2XMM survey on the basis of their high (>1) X/O and large column densities ($N_H \geq 10^{22}$ cm$^{-2}$). The sample observed with *Spitzer* has been previously investigated in other bands. The most surprising finding of the follow-up campaigns was the association of these sources with luminous near-IR objects (Mignoli et al. 2004), placing them into the class of Extremely Red Objects (EROs, $R - K \geq 5$).

The outline of the paper is as follows: in Sect. 2 we present the sample selection; *Spitzer* data reduction and analysis are discussed in Sect. 3, while in Sect. 4 we describe the analysis of the SEDs. Finally, in Sect. 5 we estimate the bolometric luminosities, the stellar masses of the host galaxies, the black hole masses, and the Eddington ratios.

Throughout this paper we adopt the "concordance" (WMAP) cosmology ($H_0$=70 km s$^{-1}$ Mpc$^{-1}$, $\Omega_M$=0.3, and $\Omega_\Lambda$=0.7; Spergel et al. 2003). Magnitudes are expressed in the Vega system.

## 2. Sample selection

The eight objects presented in this paper (see Table 1) were selected among the 10 HELLAS2XMM high X/O ratio sources detected in the $K_s$ band with ISAAC at ESO-VLT; for details on the association of the $K_s$-band counterpart to the X-ray source, see Mignoli et al. (2004). Two sources of the original sample were not selected for *Spitzer* observations: one (PKS 0537−28#31) is associated with a disky galaxy, while the other (BPM 16274#181) has an ambiguous $K_s$-band morphological classification. All but one of the sources observed by *Spitzer* belong to the first square degree field (122 X-ray sources; see Fiore et al. 2003 for the spectroscopic and photometric identification and Perola et al. 2004 for the X-ray spectral analysis); the only exception is BPM 16274#69, which belongs to the sample of the second square degree (110 X-ray sources; see Cocchia et al. 2007; Lanzuisi et al., in preparation).

[1] X/O is defined as $\log \frac{F_X}{F_R} = \log F_X + \frac{R}{2.5} + 5.5$.
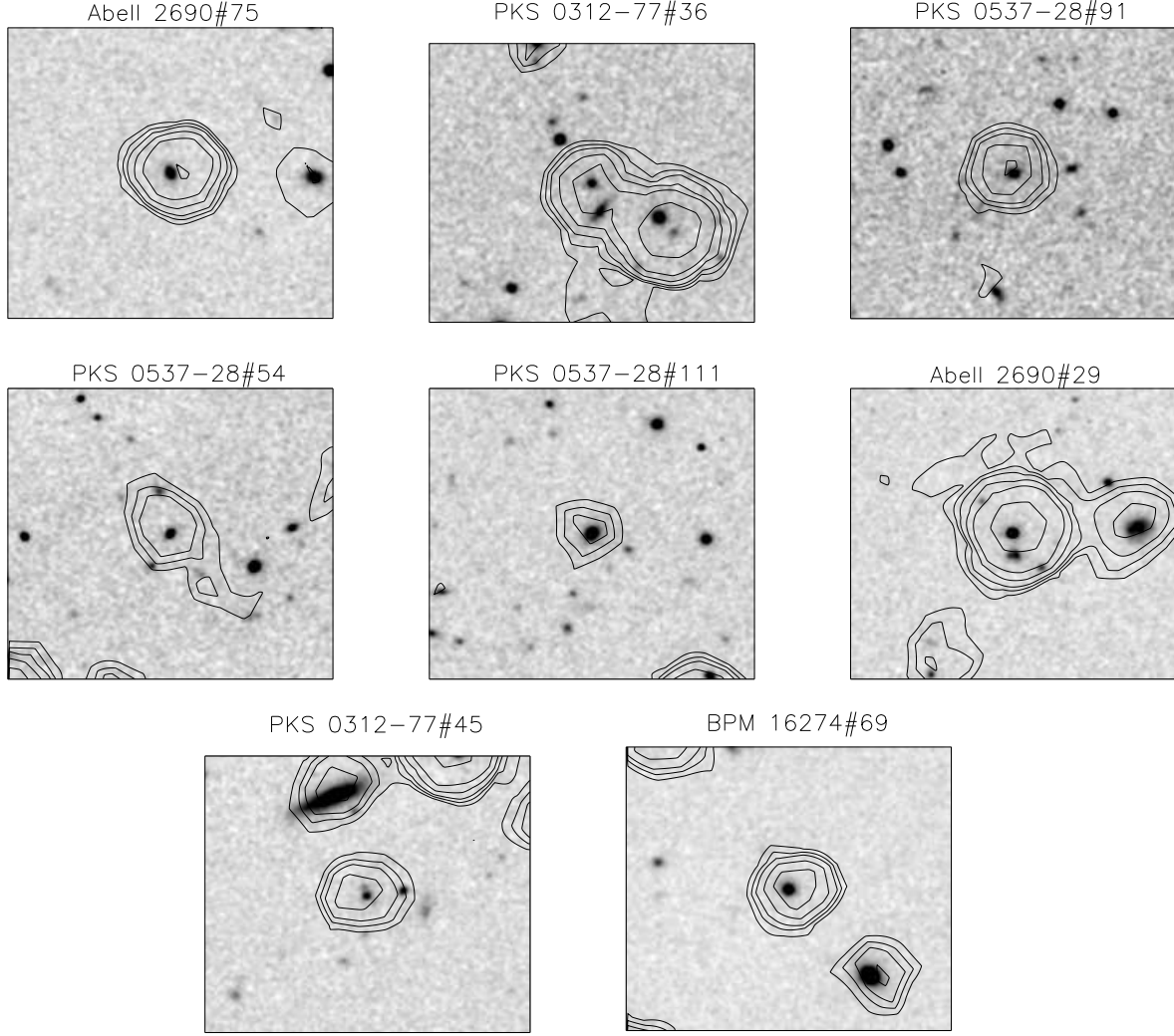
**Fig. 1.** ISAAC $K_s$ images, centered on the $K_s$ counterpart of the X-ray sources; each box is 30″ wide. North is to the top and East to the left. Contour levels of the 24 $\mu$m emission corresponding to [3, 4, 5, 7, 10, 20, 40]$\sigma$ are superimposed to each image.

The selected sources, although faint in the optical band (23.7<$R$<25.1), are all bright in the near-IR ($K_s$≲19) and, all but one, have $R - K_s > 5$, thus being EROs. Mignoli et al. (2004) were able to study the surface brightness profiles of these sources in the $K_s$ band and obtained a morphological classification. Only two sources are classified as point-like objects, while all of the others are extended, with clear detection of the host galaxy and radial profiles consistent with those of elliptical galaxies. In this latter class of sources, the central AGN is evident in the X-ray band, while in the near-IR the host galaxy dominates. An upper limit to the contribution of a central unresolved source (i.e., the nuclear emission), ranging from 2% to 12% of the galaxy emission, was obtained. Furthermore, using both the $R - K$ colour and the morphological information, a minimum photometric redshift, in the range 0.9–2.4, was estimated for these sources.

For three of the sources with the reddest colours (Abell 2690#75, Abell 2690#29 and BPM 16274#69; see Table 1), near-IR spectroscopic observations with ISAAC at ESO-VLT were performed by Maiolino et al. (2006), thus allowing for a spectroscopic identification for at least two of these sources (one redshift measurement appears tentative). The point-like source (Abell 2690#29) shows the typical rest-frame optical spectrum of high-redshift dust-reddened quasars, with a broad H$\alpha$ line (Gregg et al. 2002). The other two observed sources, both of them extended in the $K_s$ band, have narrow emission-line spectra: one is a LINER-like object at $z$=1.35 and the second source has a spectrum with a single weak line, tentatively associated with H$\alpha$ at $z$=2.13. Consistently with the morphological information, in the first source the AGN dominates the emission, while in the other two sources the nuclear spectrum is heavily diluted by the host galaxy starlight.

**Table 2.** *Spitzer* flux densities

| Source Id. | $3.6\,\mu$m $S_\nu \pm \Delta S_\nu$ | $4.5\,\mu$m $S_\nu \pm \Delta S_\nu$ | $5.8\,\mu$m $S_\nu \pm \Delta S_\nu$ | $8.0\,\mu$m $S_\nu \pm \Delta S_\nu$ | $24\,\mu$m $S_\nu \pm \Delta S_\nu$ |
|---|---|---|---|---|---|
| Abell 2690#75 | 51 ± 5 | 56 ± 6 | 89 ± 11 | 139 ± 15 | 565 ± 62 |
| PKS 0312−77#36 | 41 ± 4 | 44 ± 5 | 40 ± 8 | 71 ± 9 | 236 ± 30[a] |
| PKS 0537−28#91 | 28 ± 4 | 35 ± 4 | 42 ± 8 | 80 ± 10 | 301 ± 40 |
| PKS 0537−28#54 | 31 ± 4 | 35 ± 4 | 50 ± 10 | 47 ± 8 | 279 ± 45 |
| PKS 0537−28#111 | 88 ± 9 | 75 ± 8 | 41 ± 6 | 46 ± 7 | 148 ± 28 |
| Abell 2690#29 | 141 ± 14 | 185 ± 19 | 260 ± 27 | 371 ± 38 | 1012 ±106[a] |
| PKS 0312−77#45 | 50 ± 6 | 62 ± 7 | 69 ± 10 | 78 ± 10 | 249 ± 35 |
| BPM 16274#69 | 86 ± 9 | 92 ± 9 | 97 ± 11 | 120 ± 13 | 286 ± 34 |

The flux density is reported in units of $\mu$Jy. [a] The 24 $\mu$m flux density is probably over-estimated due to contamination from nearby sources and should be considered as an upper limit.

## 3. Spitzer observations and data reduction

The whole sample of eight hard X-ray selected sources has been observed by *Spitzer* (Werner et al. 2004), with IRAC (Fazio et al. 2004) observations of 480 s integration time and MIPS (Rieke et al. 2004) observations at 24 $\mu$m with a total integration time of $\approx$ 1400 s per position. IRAC observations were performed in photometry mode with frame time of 30 s and dither pattern of 16 points. The MIPS 24 $\mu$m observations were performed in MIPS photometry mode with frame time of 10 s, 10 cycles and small-field pattern. To reduce overheads, the cluster option was used when possible.

For the IRAC bands, we used the final combined post-basic calibrated data (BCD) mosaics produced by the *Spitzer* Science Center (SSC) pipeline (Version S12.0–S13.01). At 24 $\mu$m, we started the analysis from the BCD produced by the SSC pipeline (Version S12.4.2–S13.01) and then we applied *ad hoc* procedures to optimize the reduction, since some of our sources were close to the detection limit (see Table 2). We remind that BCD are individual frames already corrected for dark, flat field and geometric distortion. We improved the quality of the BCD by correcting each individual BCD for a residual flat field depending on the scan mirror position (Fadda et al. 2006). The residual flat fielding was obtained from our own data by averaging the BCD corresponding to the same scan mirror position and the same Astronomical Observation Request (AOR), considering all the different cluster positions. To each BCD, its median level was subtracted before this operation. This procedure was possible since our observations are not dominated by background fluctuations. The corrected BCD were co-added and background-subtracted using the SSC MOPEX software (Makovoz & Marleau 2005). The resulting mosaics were made with 2.4″ pixel size. The overall analysis at 24 $\mu$m produces mosaics with a typical noise of $\approx$ 0.020 MJy/pixel (a factor of 2 lower in comparison with the SSC pipeline mosaics). The noise map has been computed for each mosaic by scaling the measured mean *rms* of the central part of the map according to the inverse square root of the coverage map.

The flux densities of our targets in IRAC and MIPS bands were measured on the signal maps using aperture photometry at the position of the sources. The chosen aperture radius for the IRAC bands is 2.45″ and the adopted factors for the aperture corrections are 1.21, 1.23, 1.38 and 1.58 (following the IRAC Data Handbook, Version 3.0) at 3.6 $\mu$m, 4.5 $\mu$m, 5.8 $\mu$m and 8 $\mu$m, respectively.

The chosen aperture radius at 24 $\mu$m is 7.5″; aperture corrections were derived by examining the photometry of bright stars. Taking into account an additional correction of 1.15 to match the procedure used by the MIPS instrument team to derive calibration factors from standard star observations, the resulting aperture correction is 1.57 (in agreement with the SWIRE team, see Surace et al. 2005).

Table 2 reports the results of the *Spitzer* observations. To compute the photometric uncertainties, we added in quadrature the noise map and the systematic uncertainties ($\approx$10%, see MIPS and IRAC Data Handbook 2006, Version 3.0). The relative photometric uncertainties range from $\approx$10% in the best cases (IRAC channels 1 and 2), up to $\approx$20% at 24 $\mu$m in the worst ones.

All of the eight sources are clearly detected in both IRAC and MIPS 24 $\mu$m bands. At 24 $\mu$m, the flux densities span an order of magnitude, ranging between $\approx$1000 $\mu$Jy and $\approx$150 $\mu$Jy, with the faintest source (PKS 0537−28#111) close to the $5\sigma$ detection level.

In Fig. 1 the $K_s$-band images, along with the contour levels of the 24 $\mu$m emission, are shown. At 24 $\mu$m, the sources PKS 0312−77#36 and Abell 2690#29 appear to be confused. In particular, in both cases, there is a second source at $\approx$ 8-10″, unrelated to the targets. The contribution of these sources to the 24 $\mu$m flux density of our targets has been estimated by a decomposition analysis (using the PSF fitting algorithm IMFIT within the AIPS environment). Furthermore, both the sources PKS 0312−77#36 and Abell 2690#29 present a second object at $\approx$ 2″, clearly visible in the $K_s$ images, too close to our targets for a decomposition analysis, given the 24 $\mu$m pixel size. Since these close companions become increasingly fainter moving from the $K_s$ bands to the longer IRAC wavelengths, we have attributed the entire flux density estimated from the decomposition analysis to our targets (see Table 2). However, the 24 $\mu$m flux densities for these two sources should be treated as upper limits (see Fig. 2).

We point out that the deblending procedure measures the peak flux density. To convert the peak flux density into total flux density, we have assumed that the deblended objects are point-like sources and applied a correction factor of 8.9 derived from the 24 $\mu$m *Spitzer* PSF and including the 1.15 calibration factor.

## 4. Analysis of the spectral energy distributions

In this section we provide an analysis of the SEDs of our sources, in order to derive the energy distribution of the nuclear component "cleaned" by the host galaxy contribution. As anticipated in Sect. 1, the determination of the nuclear SEDs over a large wavelength range is an essential step to estimate the physical properties of the black hole, such as its bolometric luminosity, mass, and accretion rate. Taking advantage of the new *Spitzer* photometric points, simultaneously to the SED determination we have estimated the photometric redshifts of our sources. These new values are then compared with the minimum redshifts estimated by Mignoli et al. (2004) using only the $R$ and $K_s$ bands and with the spectroscopic ones measured in three cases by Maiolino et al. (2006, see §2).

Given the different morphological properties of our sources, two approaches have been adopted, one for the sources dominated in the $K_s$ band by the host galaxy (elliptical-like sources) and another one for the sources dominated by the nuclear component (point-like sources).

### 4.1. Elliptical-like sources

From the $K_s$-band morphological analysis, we know that at least up to the observed 2.2 $\mu$m band the stellar contribution dominates the emission in these sources. At longer wavelengths, the nuclear component is expected to arise as reprocessed radiation of the primary emission, while the stellar component is expected to drop (e.g., Bruzual & Charlot 2003; Silva et al. 2004).

In the analysis presented in this work, we have decided to follow a phenomenological approach, checking whether the emission of our sources can be reproduced as the sum of two components, one from the host galaxy and the other related to the reprocessing of the nuclear emission by the dusty torus envisaged by unification schemes (Antonucci 1993). The shape and relative strengths of the two components have to be consistent with all our observed data sets (multi-band photometry, $K_s$-band morphology and magnitude, $K_s$-band upper limit on the nuclear component, and X-ray spectral analysis).

For the galaxy component, we adopted a set of six galaxy templates, obtained from the synthetic spectra of GISSEL 2003 (Bruzual & Charlot 2003) assuming a simple stellar population and spanning a wide range of ages, from 1 Gyr up to a "maximum age" model ($z_{form} = 20$). The "maximum age" model has been adopted by Mignoli et al. (2004) to derive the minimum photometric redshift for the sources of the current sample.

For the nuclear component, we adopted the nuclear templates from Silva et al. (2004), based on the radiative transfer models of Granato & Danese (1994). We chose these templates since in the work of Silva et al. (2004) the radiative transfer

models are used to interpolate the observed nuclear IR data for a sizable sample of local AGN. We must note, however, that the nuclear observed SEDs are available only in the 2–20 $\mu$m regime, where data from small-aperture instruments are available. At wavelengths above $\approx 20$ $\mu$m, the SEDs are model extrapolations.

Silva et al. (2004) found that the nuclear SEDs can be expressed as a function of two parameters, the hard X-ray (2–10 keV) intrinsic luminosity, which provides the normalization to the SED, and the column density $N_H$, which gives the shape to the SED (see Fig. 2 in Silva et al. 2004). The shapes of the SEDs of the Seyfert galaxies are assumed to be valid also at quasar luminosities.

In the attempt to provide a better estimate for the source redshifts, we used the four torus templates as given by Silva et al. (2004), which depend on the column densities $N_H$, and we left the normalizations free to vary. The redshift interval explored by this procedure is 0.5–3.0; the best-fit solution is obtained when the algorithm, based on the $\chi^2$, finds a minimum in the galaxy template, torus template and redshift parameter space.

For four out of six sources the procedure finds a clear minimum $\chi^2$, which allows us to determine a photometric redshift with relatively good accuracy (see Table 3). For sources BPM 16274#69 and PKS 0537−28#54, our procedure constrains only the lower bound of the redshift interval. For all the six sources, the estimated redshifts are consistent with the minimum redshifts of Mignoli et al. (2004). In case of the source BPM 16274#69, where a secure spectroscopic redshift is available, the minimum photometric redshift ($z_{phot} > 1.25$) is consistent with the spectroscopic one ($z = 1.35$). For source Abell 2690#75, we find $z_{phot} = 1.30^{+0.30}_{-0.20}$, which is significantly lower than the spectroscopic value ($z = 2.13$) reported by Maiolino et al. (2006). In this case, we choose to adopt the photometric determination, since the spectroscopic redshift is based on the tentative detection of a single line.

The results of the SED fitting and decomposition are shown in Fig. 2. The dot-dashed line represents the best-fit galaxy template, the dashed line is the best-fit nuclear template and the thick solid line is the sum of the two components. The best-fit galaxy templates are all typical of early-type galaxies with ages between 3 and 6 Gyr. We find an overall agreement between the SED templates and the data points. Moreover, in all but one of the sources, the nuclear component derived from the best fit is consistent with the upper limits derived from the analysis of the $K_s$-band images (shown as downward-pointing arrows). In Fig. 2 we also report as dotted line the SED of the nuclear component normalized to the intrinsic (i.e., de-absorbed) X-ray luminosity following the prescriptions of Silva et al. (2004), where, at a given $N_H$, the normalization depends only on the intrinsic hard X-ray luminosity. The overall agreement between the SEDs normalized to the X-ray luminosity and the best-fit SEDs is extremely interesting, being consistent within a factor of $\approx 2$–3.

In Table 3 we report, along with the photometric redshifts, the column densities $N_H$ and the de-absorbed $L_{2-10\ keV}$ luminosities. We derive rest-frame $N_H$ column densities in the range $10^{22.0}$–$10^{23.4}$ cm$^{-2}$ and 2–10 keV luminosities in the range
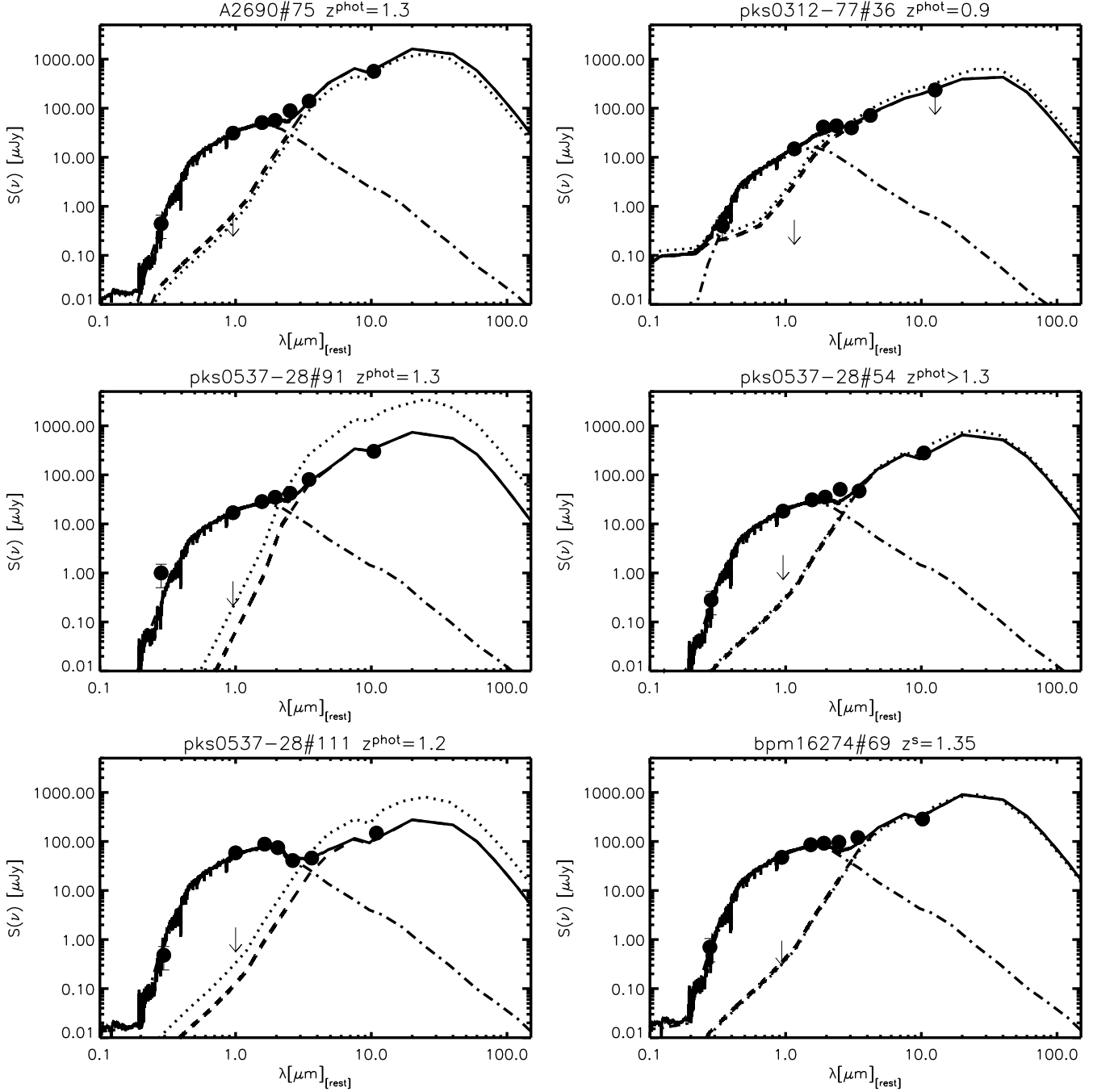
**Fig. 2.** Rest-frame SEDs of the elliptical sources (black filled circles) compared with the best-fit model obtained as the sum (solid line) of an early-type galaxy (dot-dashed line) and a nuclear component (dashed line). For comparison, the nuclear component as derived from the X-ray normalization is also reported (dotted line). The nuclear $K_s$-band upper limits (downward-pointing arrows) were derived from the morphological analysis carried out by Mignoli et al. (2004). The 24 $\mu$m upper limit of source PKS 0312−77#36 takes into account a possible contribution from a companion source. $z^s$ means that the redshift is spectroscopic (see §2 for details), while $z^{phot}$ means that the redshift is photometric (see §4.1).

$10^{43.8}$–$10^{44.7}$ erg s$^{-1}$, placing these sources among the Type 2 quasar population.

### 4.2. Point-like sources

From the $K_s$-band morphological analysis, Abell 2690#29 and PKS 0312−77#45 (see Mignoli et al. 2004 and Table 1) show

a completely different appearance at 2.2 $\mu$m in comparison with the sample of extended objects; these two sources have their near-IR emission mostly dominated by an unresolved source. The dominant role played by the AGN is supported for Abell 2690#29 also by its near-IR spectrum, where a broad H$\alpha$ emission line is detected (see Maiolino et al. 2006 and §2).
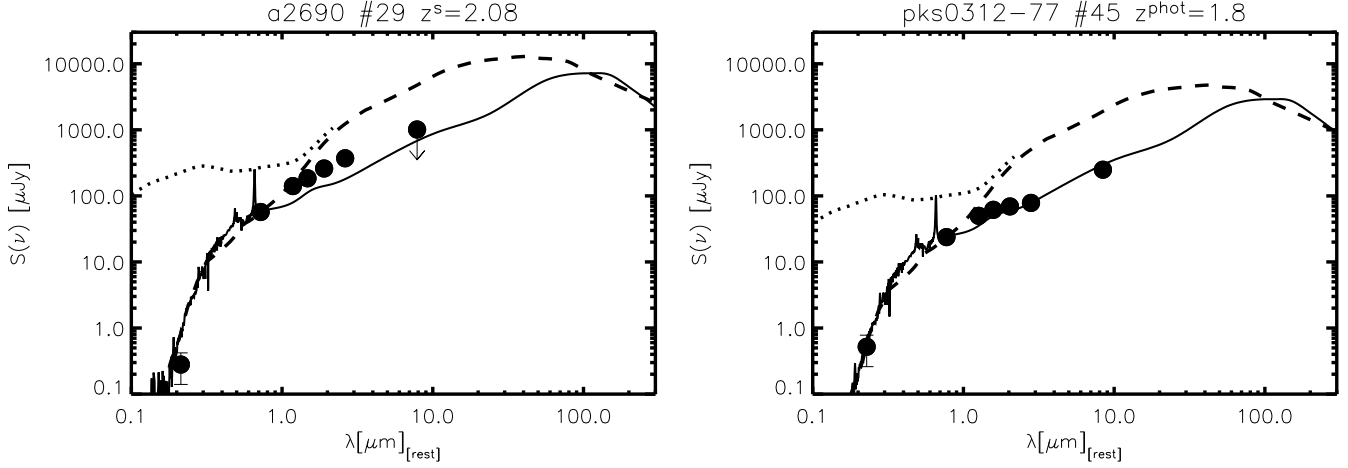
**Fig. 3.** Rest-frame SEDs of the two point-like sources (black filled circles) compared to an extinguished quasar template (dashed line) and the best-fit red quasar template (solid line). The extinguished quasar template is obtained from the unobscured quasar template of Elvis et al. (1994) using the SMC extinction law with $E(B - V) = 0.7$ and scaled to fit the $R - K_s$ colour (for comparison, the unobscured quasar template is also shown as a dotted line). The red quasar template is taken from Polletta et al. (2006). The 24 $\mu$m flux density upper limit for the source Abell 2690#29 takes into account a possible contribution from a companion source. $z^s$ means that the redshift is spectroscopic (see §2 for details), while $z^{phot}$ means that the redshift is photometric (see §4.2).

Unfortunately, the near-IR spectroscopy information is absent for PKS 0312−77#45 (see Table 1).

We first tried to reproduce their observed SEDs by reddening the composite template spectrum of bright Type 1 quasars of Elvis et al. (1994) with several extinction laws. Reddening has been applied as prescribed by Calzetti (1997) for a dust-screen model and by Pei (1992) for the Small Magellanic Cloud (SMC) galaxy. The two prescriptions produce similar effects at $\lambda > 0.5$ $\mu$m, but the SMC law produces redder spectra at shorter wavelengths for the same amount of extinction. Reddened templates with an SMC law reproduce quite well the optical spectra of dust-reddened quasars in the Sloan Digital Sky Survey (SDSS; see Richards et al. 2003), while, using the Calzetti (1997) law, Polletta et al. (2006) were able to reproduce the SEDs of X-ray sources in the *Spitzer* SWIRE survey.

The procedure of reddening a typical Type 1 quasar does not provide a satisfactory fit to the photometric data points of our sources. In Fig. 3 we show the results obtained when the prescription of Mignoli et al. (2004) for the extinction [SMC extinction law and $E(B - V) = 0.7$] is adopted.

The dashed line shows the reddened quasar template normalized to fit the $R - K_s$ colour. For comparison, the unobscured quasar template is also shown (dotted line). Although the $R - K_s$ colour is obviously reproduced, the overall SED is not well reproduced, since the observed IRAC and 24 $\mu$m flux densities are systematically lower than predicted (up to a factor of 10 at 24 $\mu$m).

The discrepancy between the data points and the reddened Type 1 quasar template might be due to the application to active galactic nuclei of an extinction curve derived from galaxies. The different behaviour of AGNs from galaxies can be attributed to different dust distribution (i.e., torus shape in AGNs), and gas-to-dust ratios, which can lead to an unusual dust reddening curve for AGNs.

Since a reddened quasar template does not reproduce the shape of our data, we adopted the red quasar template from Polletta et al. (2006), which is a composite spectrum: in the optical/near-IR band, it is the spectrum of the red quasar FIRST J013435.7−093102 from Gregg et al. (2002), while the average of several bright quasars from the Palomar-Green (PG) sample (Schmidt & Green 1983) with consistent optical data has been used in the IR. The Polletta et al. (2006) template reproduces the observed data points significantly better, allowing for the observed sharp decrease from 0.2 to 0.7 $\mu$m in the source rest frame (see Fig. 3 where the Polletta et al. 2006 spectrum is shown as a solid line).

For source Abell 2690#29, which has a spectroscopic redshift, the SED normalization has been obtained through a best-fit procedure. For source PKS 0312−77#45, where only a minimum redshift was available prior to this analysis, we have left free to vary both the normalization and the redshift.

In Table 3 we report the derived redshifts, column densities $N_H$ and de-absorbed $L_{2-10 \ keV}$ also for these sources which, similarly to the elliptical-like sources, belong to the Type 2 quasar population.

## 5. Physical parameters

### 5.1. Bolometric correction

Once the SED of the nuclear component has been determined, the following step is to estimate the bolometric luminosity $L_{bol}$, which is a quantity directly related to the central black hole activity.

The bolometric luminosity $L_{bol}$ can be estimated from the luminosity in a given band $b$, $L_b$, by applying a suitable bolometric correction $k_{bol,b} = L_{bol}/L_b$. For the X-ray selected sources, the bolometric luminosity is typically estimated

from the luminosity in the 2–10 keV band ($k_{bol,2-10\ keV} = L_{bol}/L_{2-10\ keV}$). In previous works, several authors used the bolometric correction obtained by Elvis et al. (1994) for luminous, mostly nearby quasars, i.e., $k_{bol,2-10\ keV} \approx 30$. However, these corrections could be affected by the following uncertainties: firstly, they are average corrections obtained from a few dozens of bright quasars; secondly, as discussed in Marconi et al. (2004), these corrections could overestimate the bolometric luminosities since they are based on the integral of the observed SEDs of bright unobscured AGN, without removing the IR bump (hence counting twice a fraction of $\approx 30\%$ of the intrinsic optical–UV radiation). At lower luminosities (typical of Seyfert galaxies, i.e., $10^{42} - 10^{44}$ erg s$^{-1}$), a lower value for this correction ($k_{bol,2-10\ keV} \approx 10$) was suggested (e.g., Fabian 2004). For heavily obscured luminous sources, only few objects have been studied in detail; in particular, for two SWIRE Compton-thick (i.e., log $N_H \gtrsim 24$ cm$^{-2}$) AGN Polletta et al. (2006) found $k_{bol,0.3-8\ keV} \approx 3$ and $\approx 100$.

In this work, thanks to the multi-band observations and efforts in disentangling the AGN and the host components, we try to derive directly the nuclear bolometric luminosity of our sources without assuming any average correction. We estimate $L_{bol}$ by adding the X-ray luminosity integrated over the entire X-ray range ($L_{0.5-500\ keV}$, not corrected for absorption) to the IR luminosity ($L_{1-1000\ \mu m}$).

$L_{0.5-500\ keV}$ has been estimated from the observed $L_{2-10\ keV}$ luminosity assuming a single power-law spectrum with $\Gamma=1.9$ (typical for AGN emission; see, e.g., Fig. 6 of Vignali et al. 2005 and references therein) plus absorption (where the column densities are taken from the X-ray spectral analysis; see Perola et al. 2004 and Lanzuisi et al., in preparation) and an exponential cut-off at 200 keV. The median value found for the ratio $L_{0.5-500\ keV}/L_{2-10\ keV}$ is $\approx 4$. The IR luminosity has been estimated by integrating the SED from 1 $\mu$m to 1000 $\mu$m using only the nuclear component for the AGN hosted in the elliptical galaxies (see §4.1), and the Polletta et al. (2006) template for the point-like sources.

Before computing the bolometric output of our sources, the derived IR luminosities must be properly corrected to account for the geometry of the torus and its orientation. The first correction is related to the covering factor $f$ (which represents the fraction of the primary optical–UV radiation intercepted by the torus), while the second correction is due to the anisotropy of the IR emission, which is a function of the viewing angle (see Pier & Krolik 1993 and Granato & Danese 1994 for further details).

We estimated the first correction ($\approx 1.5$) from the ratio of obscured (Compton thin + Compton thick) to unobscured quasars as required by the most recent X-ray background synthesis model (see Gilli et al. 2007) in the luminosity range of our sources. A correction of $\approx 1.5$ implies an average covering factor $f \approx 0.67$ which, in a simple torus geometry, corresponds to an angle $\theta \approx 48°$ between the perpendicular to the equatorial plane and the edge of the torus.

A first-order estimate of the anisotropy factor has been computed from the Silva et al. (2004) templates as the ratio ($R$) of the luminosity of a face-on vs. an edge-on AGN, whose obscuration is parametrized as a function of $N_H$. The integra-

tion has been performed in the 1–30 $\mu$m range, after normalizing the two SEDs to the same luminosity in the 30–100 $\mu$m range, where the anisotropy is thought to be negligible. The derived anisotropy factors are large only for the Silva et al. (2004) template with higher column density ($R \approx 3-4$ for $N_H = 10^{24.5}$ cm$^{-2}$); since all of our targets are characterized by lower obscuration, such corrections do not affect our IR luminosities significantly ($R \approx 1.2-1.3$ for $N_H \approx 10^{22.0} - 10^{23.4}$ cm$^{-2}$). In conclusion, the final combined corrections to be applied to the observed IR luminosities of our sources, given their column densities, are in the range $\approx 1.8-2.0$. After adding the X-ray luminosities, the IR correction factors would translate in a mean correction factor of $\approx 1.7$ in the computation of the bolometric luminosities.

In Table 3 the derived bolometric luminosities are reported along with the full range ($L_{0.5-500\ keV}$) of X-ray luminosities, the IR ($L_{1-1000\ \mu m}$) luminosities and the bolometric corrections ($k_{bol,2-10\ keV}$). We note that our $L_{1-1000\ \mu m}$ estimates (hence $L_{bol}$) are robust despite the choice of our SEDs. By comparing the $L_{1-1000\ \mu m}$ obtained using the Silva et al. (2004) model with the $L_{1-1000\ \mu m}$ obtained adopting other recent average quasar SEDs (i.e., Richards et al. 2006), we have verified that the uncertainties in $L_{1-1000\ \mu m}$ are within the $\approx 10\%$ level. The bolometric output of our targets is dominated by the IR reprocessed emission, the primary X-ray radiation ($L_{0.5-500\ keV}$) accounting only for $\lesssim 15\%$ of the total luminosity.

The derived median (mean) value of $k_{bol,2-10\ keV}$ is $\approx 25$ ($35 \pm 9$; see Fig. 4 and column 8 of Table 3), consistent with the value $k_{bol,2-10\ keV} \approx 30$ from Elvis et al. (1994) widely adopted in past works. However, as pointed out also by Elvis et al. (1994), the bolometric corrections span a wide range of values ($\approx 12-100$); as a consequence, the adoption of a mean value could lead to inaccurate results.

We note that in the extreme case where no corrections for the covering factor and the anisotropy of the torus are applied, we would obtain a median $k_{bol,2-10\ keV}$ of $\approx 16$.

In Fig. 4 the derived $L_{bol}$ as a function of $L_{2-10\ keV}$ is shown; the dot-dashed line joins the expected values from the analysis of Marconi et al. (2004), where $k_{bol,2-10\ keV}$ is derived by constructing an AGN reference template taking into account how the spectral index $\alpha_{ox}$ (Zamorani et al. 1981) varies as a function of the luminosity (Vignali et al. 2003). Although the bolometric luminosities estimated for our objects are on average lower than those expected on the basis of Marconi et al. (2004) relation, they are however consistent with a trend of higher $k_{bol,2-10\ keV}$ for objects with higher X-ray luminosity. If we fit our objects in the $L_{bol} - L_{2-10keV}$ plane with the same slope as the Marconi et al. (2004) relation, the difference in normalization is $\approx 50\%$.

## 5.2. Galaxy and black hole masses, and black hole Eddington ratios

For the AGN hosted in elliptical galaxies we are able to infer both the galaxy and the black hole masses. The galaxy masses are estimated, assuming a Salpeter (1955) initial mass function (IMF), from the $K_s$ luminosities taking into account that

**Table 3.** Inferred rest-frame properties of our targets

| Source Id. | $z^a$ | $N_H^b$ $(10^{22}\ \mathrm{cm}^{-2})$ | $L^c_{2-10\ keV}$ $(10^{44}\ \mathrm{erg\ s}^{-1})$ | $L^d_{0.5-500\ keV}$ $(10^{45}\ \mathrm{erg\ s}^{-1})$ | $L^e_{1-1000\ \mu m}$ $(10^{45}\ \mathrm{erg\ s}^{-1})$ | $L_{bol}$ $(10^{45}\ \mathrm{erg\ s}^{-1})$ | $L_{bol}/L_{2-10\ keV}$ | $L^f_K$ $(10^{11}\ L_{k,\odot})$ | $M_{star}$ $(10^{11}\mathrm{M}_\odot)$ | $M^g_{BH}$ $(10^9\mathrm{M}_\odot)$ | $(L_{bol}/L_{Edd})^h$ |
|---|---|---|---|---|---|---|---|---|---|---|---|
| Abell 2690#75 | $1.30^{+0.30}_{-0.20}$ | 6.9 | 3.2 | 1.3 | 9.7 | 11.0 | 34.7 | 5.2 | 3.5 | 1.3 | 0.065 |
| PKS 0312-77#36 | $0.90^{+0.05}_{-0.15}$ | 1.0 | 0.7 | 0.2 | 1.2 | 1.5 | 20.6 | 1.0 | 0.8 | 0.2 | 0.058 |
| PKS 0537-28#91 | $1.30^{+0.40}_{-0.70}$ | 25.8 | 5.3 | 2.6 | 4.4 | 7.1 | 13.4 | 2.8 | 1.5 | 0.7 | 0.084 |
| PKS 0537-28#54 | >1.30 | 1.6 | 2.0 | 0.6 | 3.9 | 4.6 | 23.0 | 3.0 | 2.0 | 0.7 | 0.049 |
| PKS 0537-28#111 | $1.20^{+0.20}_{-0.10}$ | 9.1 | 1.7 | 0.7 | 1.4 | 2.1 | 12.3 | 7.8 | 6.2 | 2.1 | 0.008 |
| Abell 2690#29 | 2.08 | 2.1 | 8.4 | 2.8 | 78.4 | 81.2 | 97.0 | 4.17 | – | – | – |
| PKS 0312-77#45 | $1.85^{+0.20}_{-0.30}$ | 8.0 | 6.2 | 2.6 | 27.2 | 29.8 | 47.9 | 1.65 | – | – | – |
| BPM 16274#69 | 1.35 | 2.5 | 2.4 | 0.8 | 5.9 | 6.7 | 28.2 | 8.8 | 6.0 | 2.5 | 0.022 |

[a] Photometric redshifts as derived from the analysis presented in this paper (see §4.1). For source PKS 0537-28#54, only a minimun redshift was estimated; for sources Abell 2690#29 and BPM 16274#69, the spectroscopic redshifts measured by Maiolino et al. (2006) are reported.

[b] The column densities, measured through X-ray spectral fitting (see Perola et al. 2004 and Lanzuisi et al., in preparation, for details), were "matched" to the redshift used in the SED best-fitting procedure (using the relation $N_H(z)=N_H(z=0)\times(1+z)^{2.6}$).
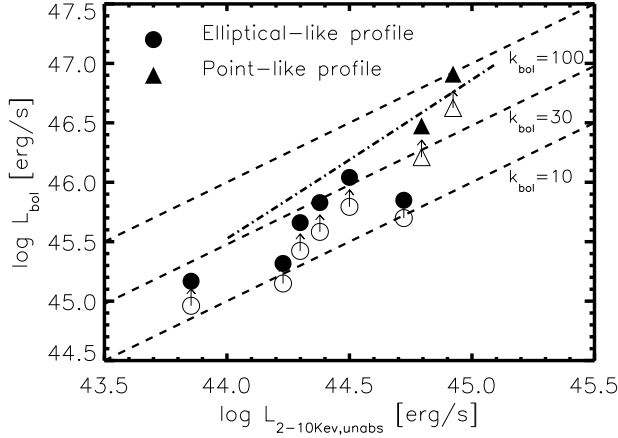
[c] Absorption-corrected X-ray luminosity.

[d] The 0.5–500 keV luminosities have been derived from the observed 2–10 keV luminosities as described in the text. The luminosities are not corrected for absorption.

[e] The 1–1000 $\mu$m luminosities have been derived from the integral of the nuclear SEDs (including the corrections described in the text). The values reported for the point-like sources refer to the Polletta et al. (2006) red quasar template (see 4.2 for details).

[f] The $K_s$-band luminosities refer to the nuclear component for the point-like sources (Abell 2690#29 and PKS 0312−77#45) and to the host-galaxy starlight for the AGN hosted in the elliptical galaxies.

[g,h] The reported $M_{BH}$ and $L_{bol}/L_{Edd}$ have been computed from the local $L_K - M_{BH}$ relation (Marconi & Hunt 2003), under the hypothesis of an evolution of the $M_{BH}/M_{star}$ ratio of a factor two with redshift (see §5.2 for details).

**Fig. 4.** Bolometric luminosity vs. absorption-corrected 2–10 keV luminosity for the six AGN hosted in the elliptical galaxies (circles) and the two point-like AGN (triangles). The filled symbols refer to the values corrected for the covering factor and torus anisotropy, while the empty symbols refer to the bolometric luminosity without applying these corrections. The dot-dashed line represents the correlation from Marconi et al. (2004). The three dashed lines represent the loci of $k_{bol,x}$=10, 30 and 100.
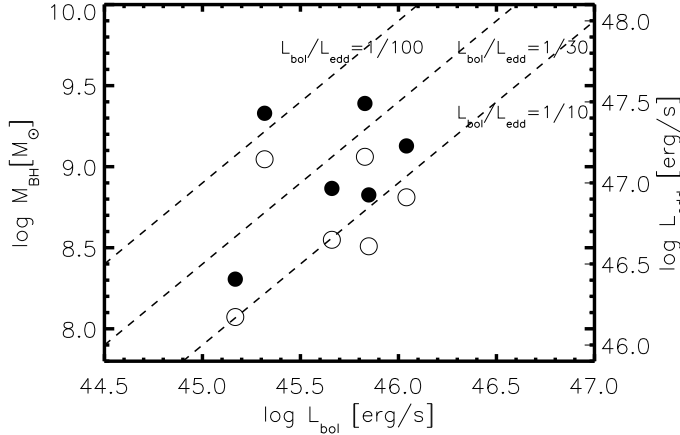


**Fig. 5.** Black hole mass ($M_{BH}$) vs. bolometric luminosity ($L_{bol}$) for the AGN hosted in the elliptical galaxies. The Eddington luminosity for a given $M_{BH}$ is reported in the right-hand axis. The black hole masses have been estimated from the local $L_K - M_{BH}$ relation (Marconi & Hunt 2003) under two different hypotheses (see 5.2): (1) evolution by a factor of two of the $M_{BH}/M_{star}$ ratio with redshift in comparison to the local values (black filled circles); (2) no evolution of the $M_{BH}/M_{star}$ ratio (empty circles). The three dashed lines represent the loci of $L_{bol}/L_{Edd} = 0.01, 0.033$ and $0.1$ (from left to right).

$M_{star}/L_K$ for an old stellar population can vary from $\approx 0.5$ to $\approx 0.9$ (for ages between 3 and 6 Gyr; Bruzual & Charlot 2003). We can derive $M_{star}$ directly from $L_K$ since for these sources the $K_s$-band emission is dominated by the galaxy starlight. The

rest-frame $L_K$ have been derived using the appropriate SED templates (see Sect. 4.1). The inferred stellar masses are in the range $(0.8–6.2)\times10^{11}$ $M_\odot$, implying that our obscured AGN are hosted by massive elliptical galaxies at high redshifts. In Table 3 both the $L_K$ and $M_{star}$ values are reported; we note that the different assumption of the Chabrier (2003) IMF would produce a factor $\approx 1.7$ lower masses (di Serego Alighieri et al. 2005).

To estimate the black hole masses, we take advantage of the local $M_{BH} - L_K$ relation (Marconi & Hunt 2003) which, taking into account the $M_{star}/L_K$ values, is expression of the intrinsic $M_{BH} - M_{star}$ relation. Given the challenging measurements of high-redshift black hole masses, the behaviour of this relation with redshift is still matter of debate and different authors, using different techniques, have found different results.

Woo et al. (2006) and Peng et al. (2006) derive a significant evolution of the $M_{BH} - M_{star}$ relation with redshift, being the $M_{BH}/M_{star}$ ratio larger, at high redshift, up to a factor $\approx 4$ in comparison to the local value. In the Woo et al. (2006) analysis the discrepancy with respect to the local value is already present at $z = 0.36$, while Peng et al. (2006) find an average $M_{BH}/M_{star}$ a factor $\gtrsim4$ times larger than the local value at $z > 1.7$, while at lower redshifts ($1 \lesssim z \lesssim 1.7$) they derive a ratio which is at most two times higher than the local value, and maybe consistent with marginal or no evolution. On the other hand, Shields et al. (2006) and Hopkins et al. (2006) suggest that the $M_{BH}/M_{star}$ ratio is not significantly higher (at most a factor of two) than that measured locally up to $z \lesssim 2$.

Given these uncertainties about the evolution of the $M_{BH} - M_{star}$ relation with redshift, we have estimated the black hole masses for our objects under two different hypotheses: (1) the $M_{BH}/M_{star}$ ratio is higher than locally by a factor two in the redshift range ($0.9 \lesssim z \lesssim 1.4$) of our sources; (2) the $M_{BH}/M_{star}$ ratio does not evolve with redshift.

In both cases, our results imply very massive black hole masses (see Fig. 5), in the range $\approx 2.0 \times 10^8 - 2.5 \times 10^9$ $M_\odot$ in the former hyphothesis, with a factor of two lower values under the second hypothesis.

Our estimated $M_{BH}$ are consistent with the results derived by McLure & Dunlop (2004) studying a large sample of Type 1 SDSS quasars and deriving the black hole masses from virial methods; most of their black hole masses are in the range $1.5\times10^8$–$2.5\times10^9$ $M_\odot$ in the redshift interval of our sample (see Fig. 1 of McLure & Dunlop 2004).

From the comparison of the bolometric luminosities computed in the previous section (see Table 3) with the Eddington luminosities calculated from the black hole masses estimated above, we derive that our obscured AGN are radiating at a relatively low fraction of their Eddington luminosity ($\lambda \approx 0.008$–$0.084$ and $\lambda \approx 0.015$–$0.170$ under the two hypotheses; see Fig. 5 and Table 3). This finding confirms and extends to a larger sample the results found by Maiolino et al. (2006) for two sources of our sample and by Brusa et al. (2005) for a sample of EROs in the "Daddi Field". As suggested by Maiolino et al. (2006), the data indicate that our very massive black holes may have already passed their rapidly accreting phase and are reaching their final masses at low accretion rates.
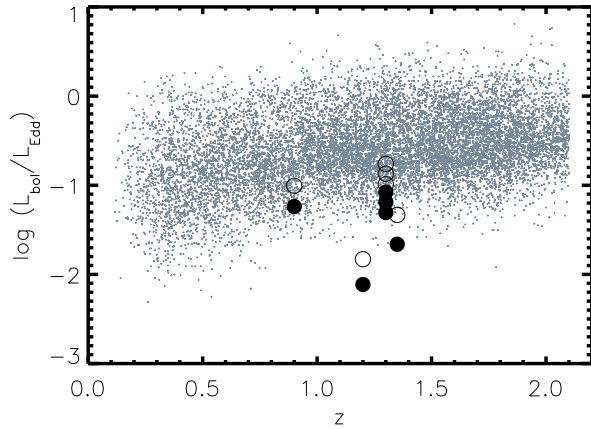
**Fig. 6.** Bolometric luminosity as a fraction of the Eddington luminosity vs. redshift for the whole sample of SDSS quasars of McLure & Dunlop (2004), plotted as small crosses. The large circles indicate the six HELLAS2XMM AGN hosted in elliptical galaxies (symbols as in Fig. 5).

The estimated radiating efficiencies are significantly lower than the average $L_{bol}/L_{Edd} \approx 0.4$ inferred by Marconi et al. (2004). However, since in the Marconi et al. (2004) model only the phases of significant black hole growth are considered, our results are not in contrast with the proposed model but suggest that our targets belong to the tail of the sources characterized by low accretion rates. Consistently, our data (black filled and empty circles representing the evolution and no-evolution hypothesis, respectively) lie in the lower envelope of the Eddington ratio distribution found by McLure & Dunlop (2004) for their large SDSS quasar sample. This is shown in Fig. 6, where our data are overlaid on the SDSS data points. This suggests that the SDSS quasar survey and the HELLAS survey probe different regimes of AGN activity: the SDSS samples the brightest sources in the sky ($R \lesssim 20$), most likely characterized by a high accretion rate, while our targets (X-ray selected, optically faint, i.e., $R > 24$, and obscured), are associated with a different evolutionary phase. We argue that the SMBH in our targets has already reached its final mass and the observed emission is witnessing a late stage of the accretion activity.

## 6. Conclusions

We have performed with *Spitzer* a pilot program to study a sample of eight Type 2 (i.e., luminous and obscured) quasars at high redshift, selected from the HELLAS2XMM survey. Three sources have a measured spectroscopic redshift (two secure and one tentative) from near-IR spectroscopy; the remaining objects have an estimated minimum redshift obtained from the $R - K$ colours. On the basis of their $K_s$-band morphological properties, the sample is divided into two classes: sources with radial profiles typical of elliptical galaxies and point-like objects. The most important results can be summarized as follows:

- All of the eight sources have been clearly detected in both IRAC and MIPS 24 $\mu$m bands.
- The *Spitzer* observations have allowed us to detect the nuclear component (often hidden at short wavelengths by the host galaxy) as thermal IR re-processed emission from the circumnuclear torus. While for the two point-like sources the nuclear component dominates at all frequencies, for the six sources with elliptical-like radial profile the contribution from the strong stellar continuum is dominant up to the first IRAC bands, but the torus emission accounts for the entire emission at 24 $\mu$m.
- Taking advantage of the new *Spitzer* data, the nuclear SEDs of the sources have been modeled and new photometric redshifts have been estimated, following two approaches: for the elliptical sources, the nuclear emission has been "cleaned" from the host galaxy contribution adopting a two-component model (galaxy plus nuclear component), constrained using all the extensive observed data sets. For the point-like sources, the SEDs appear inconsistent with an extinguished Type 1 quasar template, being well reproduced by an empirical SED of red quasars (Polletta et al. 2006). We find an overall agreement between the SED templates and the data points, and the derived photometric redshifts are consistent with the spectroscopic ones for two sources.
- Using the model components to extrapolate the nuclear SEDs in the far-IR regime, we derived the bolometric luminosities (being in the range $\approx 10^{45} - 10^{47}$ erg s$^{-1}$) by adding the IR luminosities to the full range of X-ray luminosities. In this computation, we have considered and discussed the corrections to be applied to the observed IR luminosities to take into account the covering factor of the torus and the anisotropy of the IR emission. The median 2–10 keV bolometric correction is $\approx 25$, consistent with the value typically assumed in literature.
- For the elliptical sources, thanks to the independent estimates of the stellar light and nuclear bolometric luminosity, the physical parameters of the central black holes have been estimated using the $M_{BH} - L_K$ relation and exploring different hypotheses for the evolution of the $M_{BH}/M_{star}$ ratio with redshift. Under the hyphothesis that the $M_{BH}/M_{star}$ ratio is a factor of two higher at $z \approx 1.2$ than locally, our luminous, obscured AGN have masses in the range (0.2-2.5)$\times 10^9$ $M_\odot$, reside in massive [(0.8-6.2)$\times 10^{11}$ $M_\odot$] high-redshift ellipticals and are characterized by low Eddington ratios ($\lambda \approx 0.008$–0.084). Through our direct estimate of the IR luminosity, we confirm the conclusion of Maiolino et al. (2006) that these black holes may have already passed their rapidly accretion phase.

## References

Antonucci, R. 1993, ARA&A, 31, 473

Baldi, A., Molendi, S., Comastri, A., et al. 2002, ApJ, 564, 190

Barger, A. J., Cowie, L. L., Mushotzky, R. F., et al. 2005, AJ, 129, 578

Brusa, M., Comastri, A., Daddi, E., et al. 2005, A&A, 432, 69

Bruzual, G. & Charlot, S. 2003, MNRAS, 344, 1000

Calzetti, D. 1997, in American Institute of Physics Conference Series, ed. W. H. Waller, 403

Chabrier, G. 2003, PASP, 115, 763

Cocchia, F., Fiore, F., Vignali, C., et al. 2007, A&A, in press, astro-ph/0612023

Comastri, A. & Fiore, F. 2004, Ap&SS, 294, 63

Comastri, A., Setti, G., Zamorani, G., & Hasinger, G. 1995, A&A, 296, 1

di Serego Alighieri, S., Vernet, J., Cimatti, A., et al. 2005, A&A, 442, 125

Elvis, M., Wilkes, B. J., McDowell, J. C., et al. 1994, ApJS, 95, 1

Fabian, A. C. 2004, in Coevolution of Black Holes and Galaxies, ed. L. C. Ho, 446

Fadda, D., Flores, H., Hasinger, G., et al. 2002, A&A, 383, 838

Fadda, D., Marleau, F. R., Storrie-Lombardi, L. J., et al. 2006, AJ, 131, 2859

Fazio, G. G., Hora, J. L., Allen, L. E., et al. 2004, ApJS, 154, 10

Fiore, F., Brusa, M., Cocchia, F., et al. 2003, A&A, 409, 79

Franceschini, A., Manners, J., Polletta, M. d. C., et al. 2005, AJ, 129, 2074

Gilli, R., Comastri, A., & Hasinger, G. 2007, A&A, 463, 79

Granato, G. L. & Danese, L. 1994, MNRAS, 268, 235

Granato, G. L., Danese, L., & Franceschini, A. 1997, ApJ, 486, 147

Gregg, M. D., Lacy, M., White, R. L., et al. 2002, ApJ, 564, 133

Hickox, R. C. & Markevitch, M. 2006, ApJ, 645, 95

Hopkins, P. F., Hernquist, L., Cox, T. J., et al. 2006, ApJS, 163, 1

Lonsdale, C., Polletta, M. d. C., Surace, J., et al. 2004, ApJS, 154, 54

Maiolino, R., Mignoli, M., Pozzetti, L., et al. 2006, A&A, 445, 457

Makovoz, D. & Marleau, F. R. 2005, PASP, 117, 1113

Marconi, A. & Hunt, L. K. 2003, ApJ, 589, L21

Marconi, A., Risaliti, G., Gilli, R., et al. 2004, MNRAS, 351, 169

McLure, R. J. & Dunlop, J. S. 2004, MNRAS, 352, 1390

Mignoli, M., Pozzetti, L., Comastri, A., et al. 2004, A&A, 418, 827

Pei, Y. C. 1992, ApJ, 395, 130

Peng, C. Y., Impey, C. D., Rix, H.-W., et al. 2006, ApJ, 649, 616

Perola, G. C., Puccetti, S., Fiore, F., et al. 2004, A&A, 421, 491

Pier, E. A. & Krolik, J. H. 1993, ApJ, 418, 673

Polletta, M. d. C., Wilkes, B. J., Siana, B., et al. 2006, ApJ, 642, 673

Richards, G. T., Hall, P. B., Vanden Berk, D. E., et al. 2003, AJ, 126, 1131

Richards, G. T., Lacy, M., Storrie-Lombardi, L. J., et al. 2006, ApJS, 166, 470

Rieke, G. H., Young, E. T., Engelbracht, C. W., et al. 2004, ApJS, 154, 25

Rigby, J. R., Rieke, G. H., Maiolino, R., et al. 2004, ApJS, 154, 160

Salpeter, E. E. 1955, ApJ, 121, 161

Schmidt, M. & Green, R. F. 1983, ApJ, 269, 352

Shields, G. A., Salviander, S., & Bonning, E. W. 2006, New Astronomy Review, 50, 809

Silva, L., Maiolino, R., & Granato, G. L. 2004, MNRAS, 355, 973

Soltan, A. 1982, MNRAS, 200, 115

Spergel, D. N., Verde, L., Peiris, H. V., et al. 2003, ApJS, 148, 175

Surace, J. A., Shupe, D. L., Fang, F., & et al. 2005, technical report, The SWIRE Data Release 2. Available at `http://swire.ipac.caltech.edu/swire/astronomers/publications/SWIRE2_doc_083105.pdf`

Vignali, C., Brandt, W. N., & Schneider, D. P. 2003, AJ, 125, 433

Vignali, C., Brandt, W. N., Schneider, D. P., & Kaspi, S. 2005, AJ, 129, 2519

Werner, M. W., Roellig, T. L., Low, F. J., et al. 2004, ApJS, 154, 1

Woo, J.-H., Treu, T., Malkan, M. A., & Blandford, R. D. 2006, ApJ, 645, 900

Zamorani, G., Henry, J. P., Maccacaro, T., et al. 1981, ApJ, 245, 357